Proceedings World Geothermal Congress 2000
Kyushu - Tohoku, Japan, May 28 - June 10, 2000

HYDROTHERMAL FLUID FLOW AND MINERAL ALTERATION IN A FRACTURED ROCK UNDER MULTIPHASE H_2O-CO_2 MIXTURE CONDITIONS

Tianfu Xu and Karsten Pruess
Earth Sciences Division, Lawrence Berkeley National Laboratory, University of California, Berkeley, CA 94720.

Key words: hydrothermal fluid, mineral alteration, reactive transport, fracture-matrix interaction

ABSTRACT

The geochemical evolution of hydrothermal fractured rock systems occurs through a complex interplay of multi-phase fluid and heat flow, and chemical transport processes. On the basis of previous work we present simulations of reactive hydrothermal flow that include (1) detailed fracture-matrix interaction for fluid, heat and chemical constituents, (2) gas phase participation in multiphase fluid flow and geochemical reactions, (3) heat effects on thermophysical and chemical properties and processes, and (4) the kinetics of fluid-rock chemical interaction. Results indicate that vapor-CO_2 discharges through fractures in rhyolitic caprock, cause strong alteration of the earlier formed primary minerals and lead to the formation of secondary minerals, resulting in changes in physical and chemical properties of the system.

1. INTRODUCTION

The interaction between hydrothermal fluids and the rocks through which they migrate alters the earlier formed primary minerals and leads to the formation of secondary minerals, resulting in changes in physical and chemical properties of the system. The traditional analysis of geochemical evolution and rock alteration is to separate fluid flow and chemical transport, using geochemical batch models (Henley et al., 1984; Weare, 1987; Spycher and Reed, 1989; Wolery, 1992; Moller et al., 1998). However, the geochemical evolution in hydrothermal fractured rock systems occurs through a complex interplay of multi-phase fluid and heat flow, and chemical transport processes. Recently there has been a growing interest in combining flow and transport with geochemical modeling (Steefel and Lasaga, 1994; White, 1995; White and Christenson, 1998; and White and Mroczek, 1998). On the basis of this prior work we consider the following important aspects in this study, (1) detailed fracture-matrix interaction for fluid, heat and chemical constituents, (2) gas phase participation in multiphase fluid flow and geochemical reactions, (3) heat effects on thermophysical and chemical properties and processes, and (4) the kinetics of chemical fluid-rock interaction.

The range of problems concerning the interaction of hydrothermal fluids with rocks is very broad. In the present study, we confine our attention to the evolution of geothermal fields associated with magmatic activity, such as are encountered in the Long Valley Caldera (LVC), California (Sorey, 1985; White and Peterson, 1991; Kennedy, personal comm.) and in the Taupo Volcanic Zone, New Zealand (White and Christenson, 1998). In the hydrothermal fluids in these areas, vapor and CO_2 are the dominant gas phase constituents. The present study is not specific to any geothermal field site, but reservoir conditions and some chemical data are modeled after the hydrothermal system in the LVC (Sorey, 1985; White and Peterson, 1991).

Our simulations of non-isothermal reactive chemical transport are made with the TOUGHREACT code (Xu and Pruess, 1998), which was developed by introducing reactive chemistry into the framework of the existing multi-phase fluid and heat flow code TOUGH2 (Pruess, 1991). The model uses a sequential iteration approach, which solves the transport and the reaction equations separately. The flow and transport in geologic media are based on space discretization by means of integral finite differences. An implicit time-weighting scheme is used for flow, transport, and geochemical reaction. The chemical transport equations are solved independently for each component, whereas the reaction equations are solved on a grid block basis using Newton-Raphson iteration. The model can be applied to one-, two-, or three-dimensional porous and fractured media with physical and chemical heterogeneity. The model can accommodate any number of chemical species present in liquid, gas and solid phases. Transport of aqueous and gaseous species by advection and molecular diffusion is considered in both liquid and gas phases. Aqueous complexation and gas dissolution/exsolution are considered under the local equilibrium assumption. Mineral dissolution/precipitation can proceed either subject to local equilibrium or kinetic conditions. Full details of the model are given in Xu and Pruess (1998).

If in the simulations it were possible to (a) achieve a realistic representation of all important physical and chemical processes, and (b) utilize realistic hydrogeologic and chemical parameters for the hydrothermal system under study, then the outcome of the numerical simulations should match field observations. Because of numerous uncertainties and approximations, such an ambitious goal cannot be completely reached at present. For example, the kinetics of heterogeneous reactions are scale and history-dependent, and cannot be reliably quantified. Reactive surface areas are notoriously uncertain and subject to poorly quantifiable phenomena such as armoring of mineral phases by others. Two-phase flow in fractured rock is affected by multi-scale heterogeneities. The lack of sufficiently detailed characterization data, as well as the enormous intrinsic variability of two-phase flow in fractures severely limit possibilities for a fully mechanistic description. In undertaking the simulation presented below we were mindful of these limitations and have pursued more modest objectives. Our simulation should be thought of as a "numerical experiment" which permits a detailed view of the dynamical interplay between coupled hydrologic, thermal, and chemical processes, albeit in an approximate fashion. A critical evaluation and discussion of modeling results on their own terms can provide useful insight into process mechanisms such as fracture-matrix interaction, liquid-gas phase partitioning, and conditions and parameters controlling heterogeneous reactions.

2. PROBLEM SETUP

We consider an idealized fractured rock with a set of plane, parallel vertical fracture zones at a spacing of 3.5 m. At a depth of 280 m, the fracture is charged with a vapor-CO_2 mixture from the underlying hydrothermal reservoir. Because of symmetry of this fractured rock, only one column of matrix blocks needs to be considered (Figure 1). A 1-m-thick vertical slice is modeled, where total depth of 280 m is discretized into 56 layers of 5 m thickness. The fracture is considered as one model grid zone. The rock matrix is further discretized into 6 grid zones with permeability and reactive surface area decreasing away from the fracture. A heat conductivity of 2.1 W/m^{o}C, a specific heat of 920 J/kg^{o}C, and an aqueous chemical diffusion coefficient of 1×10^{-10} m^2/s are used. Other parameters for the fracture and matrix are listed in Table 1. The top atmosphere and bottom hydrothermal reservoir are modeled as constant pressure boundaries with properties shown in Figure 1. At a depth of 87.5 m the rising hot water mixes with shallow cold meteoric aquifer water. The cold water (11 ^{o}C) recharge is assumed to occur only in the fracture portion at a rate of 3×10^{-5} kg/s, and is treated as a source term for fluid, heat and chemical constituents, the concentrations of which are given in Table 2.

The reservoir chemical composition is based on data reported by White and Peterson for Long Valley (1991). The major chemical species in the Wells MBP-1, MBP-3, RDO-8, and 44-16 fluids are in general similar, and we use Well RDO-8 measured chemical data (Table 2) for our simulation. CO_2 is the dominant gaseous species in the hydrothermal system, and its partial pressures range from 1 to 9 bar. We use an intermediate partial pressure value of 3.964 bar. The cold recharge water chemical composition is taken from Sorey (1985) for cold Big Springs of LVC (Table 2) which is assumed to be representative of the shallow aquifer meteoric water. Thermodynamic equilibrium constants are taken from the EQ3/6 database (Wolery, 1992).

For the purpose of our study, we chose an initial rock mineral assemblage as listed in Table 3, which is based on the studies carried out by Steefel and Lasaga (1994) and White and Christenson (1998). The dissolution of the primary minerals is kinetically controlled. The kinetic rate law (Steefel and Lasaga, 1994) used is

$$r_m = A_m\, k_m\left[1-\left(\frac{Q_m}{K_m}\right)\right] \qquad (1)$$

where m is mineral index, r_m is the dissolution/precipitation rate (positive values indicate dissolution, and negative values precipitation), A_m is the specific reactive surface area per kg H_2O, k_m is the rate constant (moles per unit mineral surface area and unit time) which is temperature dependent, K_m is the equilibrium constant for the mineral-water reaction of mineral m, and Q_m is ion activity product. The temperature dependence of the reaction rate constant is expressed via an Arrhenius equation (Steefel and Lasaga, 1994),

$$k = k_{25}\exp\left[\frac{-E_a}{R}\left(\frac{1}{T}-\frac{1}{298.15}\right)\right] \qquad (2)$$

where E_a is the activation energy, k_{25} is the rate constant at 25 ^{o}C, R is gas constant, and T is absolute temperature. The initial specific surface areas given in Table 3 must be multiplied by the reactive surface area factor given in Table 1 for different matrix grid zones. The precipitation of secondary minerals (Table 3) is represented using the same kinetic expression as that for dissolution. The rates of precipitation of all secondary minerals are assumed to be the same as dissolution kinetic constants. A constant reactive surface area of 0.01 m^2 per one dm^3 (cubic decimeter) medium is used.

The simulation is run for 1000 years. During this period of time, we assume there is no significant permeability change due to mineral dissolution and precipitation. Initially, we perform a fluid and heat flow simulation until a steady-state is attained. Then we simulate chemical transport and fluid-rock interactions using the steady-state fluid and heat flow as the initial condition. The described two-step approach can give a detailed description of chemical evolution of the system at a reduced computational expense. Despite our use of a two-step approach, our model is fully capable of simulating both flow and reactive transport at the same time. We should point out that CO_2 consumed by mineral precipitation such as calcite is assumed not to affect its partial pressure (Pco2) and then fluid flow. If at the bottom boundary (geothermal reservoir) Pco2 holds constant as the case simulated in this paper, this assumption is justified. A 1-D vertical column is tested first with the bottom and top boundary conditions as shown in Figure 1. The effect of CO_2 consumed by calcite precipitation on fluid flow is negligible in this kinetically-controlled chemical system. Most calcite precipitation occurs close to the bottom reservoir. CO_2 consumed by calcite precipitation is replenished by enhanced physical transport processes from the reservoir.

3. RESULTS AND DISCUSSION

3.1. Fluid flow and heat transfer

The contour plots of liquid water saturation and CO_2 partial pressure are presented in Figure 2. The tight rock matrix is almost water saturated due to high capillary suction effect, and therefore gas (vapor and CO_2) access to the matrix is impeded. At a depth of 87.5 m, the matrix is highly saturated with water. This is because the fracture receives a lateral cold water recharge, some of which is immediately imbibed by the matrix, with the remainder flowing upward along the fracture. High liquid saturation close to the land surface is due to condensation from heat loss to the atmosphere (13 ^{o}C). The temperature distribution is quite uniform between fracture and matrix, since conduction is the dominant heat transfer process and the two media are almost homogeneous in terms of their thermal properties. Figure 3 gives a more detailed evolution along the vertical fracture. The liquid water saturation decreases slightly with increasing elevation until a depth of 87.5 m, where it increases dramatically due to the cold water recharge. It then again decreases slightly, and finally increases due to condensation from heat loss to the land surface. The relative liquid flow rate (R_L), normalized to the total (fracture and matrix) land surface discharge (5.49×10^{-5} kg/s), slightly decreases from the bottom like the liquid saturation. After the cold water recharge, R_L dramatically increases from 24% to 87%. In addition, almost the total CO_2 output (2.46×10^{-6} kg/s) discharges from the fracture. Gas phase pressure gradually decreases from the bottom to the top, and in the matrix is slightly greater than that in the fracture. Figure 2b shows the contour plots of CO_2 partial pressure (Pco2, in bar) that generally decreases from the bottom to the top but a peak value

appears after mixing with cold water (this can be clearly seen from Figure 3b). This sharp increase of Pco2 is because (1) gas saturation is dramatically decreased due to the cold water recharge, (2) cooling and condensation causes CO_2 to become the dominant gas phase constituent, and (3) CO_2 solubility in water has a minimum at 160 ^oC (Battistelli et al., 1997), the temperature in the mixing zone. In reality, this increase is achieved gradually since cold water recharge is applied over a longer depth rather than one grid block (5 m depth) used in the simulation.

3.2. Rock alteration

We express rock alteration in terms of change of mineral volume fraction that is dimensionless, as porosity. The sum of all mineral abundances and porosity is equal to unity, and the sum of their (minerals and porosity) changes equals zero. Negative values of the abundance changes indicate dissolution, while positive indicate precipitation. Contour plots for changes of some mineral abundances after 1000 years are presented in Figure 4. K-feldspar dissolution patterns (Figure 4a) show two peaks, one is after the mixing, and the other is close to the bottom. Significant dissolution of K-feldspar and albite after the mixing can be clearly seen from the profile along the fracture (Figure 5a). This is because: (1) SiO_2(aq), Na, and K concentrations in cold meteoric water (see Table 2) are lower, and (2) solubilities of minerals in the mixed water are much larger than in the cold water (the temperature of the mixture is approximately 160 ^oC, and cold water 11 ^oC). In addition, cristobalite and anorthite dissolution decreases from the bottom to top. After mixing with cold water, their dissolution decreases significantly. Ca^{2+} released from dissolution of anorthite is taken up by calcite precipitation (Figure 4b). Calcite precipitation decreases from the bottom until the mixing horizon. This is because (1) calcite solubility increases with decreasing temperature, and (2) Ca^{2+} availability decreases because less anorthite dissolves at shallower elevations. Calcite precipitation occurs mainly in the fracture, and gradually decreases away from the fracture in the matrix interior. Kaolinite precipitation (Figure 4c) occurs mostly in the lower temperature range, and concentrates around the mixing horizon. Muscovite and paragonite are also formed as secondary phases. Precipitation of these minerals generally decreases from the bottom to the top. Muscovite precipitation is extensive, and decreases gradually from the fracture to the matrix interior. Finally, some amorphous silica precipitates close to the land surface.

Figure 6 shows an increasing porosity (from t=0) at deeper elevations. The maximum increase in porosity appears in the matrix close to the fracture wall, not on the fracture walls. This indicates that there is considerable dissolution in the matrix. The dissolved products in the matrix are transported locally by diffusion to the fracture, then the chemical components leached from the matrix are transported upward through the fracture. A significant porosity increase also occurs in the mixing region. Figure 5b shows in detail the porosity evolution along the fracture. Three regions of change can be distinguished. The porosity increases at depth, and then decreases as the mixing horizon is approached. A larger porosity increase (with a maximum value of 0.8%) occurs after mixing with cold meteoric water. The pattern of porosity change in the fracture suggests that: (1) close to the heat source dissolution dominates over precipitation due to the higher temperature, (2) away from the heat source precipitation dominates, because chemical components transported from the bottom precipitate in a lower temperature environment, and (3) the mixing with cold and dilute meteoric water results in an enhanced dissolution.

Estimates of field mineral dissolution and precipitation rates cover a wide range of values. Specific reactive surface areas may vary over several orders of magnitude (White and Peterson, 1990). For the purpose of sensitivity analysis, we performed two additional simulations by increasing and decreasing the surface areas listed in Table 3 by one order of magnitude. A surface area increase results in more dissolution and more porosity increase in the matrix, while a decrease causes less dissolution in the matrix and slightly enhanced dissolution in the fracture.

CO_2 outflow is frequently observed in hydrothermal fields such as in LVC. The simulated calcite precipitation in the high temperature fracture region agrees with field observations. Calcite is the dominant secondary mineral observed in well cuttings and cores from hydrothermal fields associated with magmatic activity (White and Peterson, 1991). Calcite precipitation in a fracture may inhibit fluid flow and chemical transport, and stop fracture fluid and chemical exchange with the matrix. These effects are not considered in the present simulation. Kaolinite precipitation occurs mostly in the lower temperature range, and concentrates around the mixing horizon. This pattern is consistent with field observations reported by Flexser (1991).

4. CONCLUDING REMARKS

The fracture is the dominant global fluid flow and chemical transport pathway. The matrix serves as a high capacity heat buffer and transfer medium due to its larger volume, and as a local medium for chemical diffusion. Almost all CO_2 is transported through the fracture. Cooling and condensation results in an elevated CO_2 partial pressure. The CO_2 is the dominant gas phase constituent close to the land surface. Local chemical diffusive transport from the matrix to the fracture plays an important role in mineral dissolution and precipitation. Considerable dissolution in the matrix is observed over a 1000 year time period. The dissolved chemical constituents leached from the matrix are transported upward through the fracture. Close to the heat source dissolution dominates over precipitation, resulting in increasing porosity. Away from the heat source precipitation dominates because chemical constituents transported from the bottom, precipitate in a lower temperature environment. Mixing with cold and dilute meteoric water also results in enhanced dissolution, and porosity increase.

The predicted alteration of primary rock minerals and the development of secondary mineral assemblages are consistent with field observations such as in LVC. The rock alteration pattern is sensitive to the reactive surface areas which in turn affect the reaction rates. A surface area increase results in more dissolution and more porosity increase in the matrix, while a decrease causes less dissolution in the matrix and slightly enhanced dissolution in the fracture. The model presented here may allow for testing production scenarios near a heat-source and in cold meteoric water mixing environments.

ACKNOWLEDGEMENTS

We thank John Apps for helpful discussions and suggestions. We are grateful to Nicolas Spycher, Mack Kennedy, Curtis Oldenburg, Steve White, and Daniel Swenson for a review of the manuscript and suggestions for improvement. This work was supported by the Laboratory Directed Research and Development Program of the Ernest Orlando Lawrence Berkeley National Laboratory, and by the Assistant Secretary for Energy Efficiency and Renewable Energy, Office of Geothermal and Wind Technologies, of the U.S. Department of Energy, under Contract No. DE-AC03-76SF00098.

REFERENCES

Battistelli, A., Calore, C., and Pruess, K. (1997). The Simulator TOUGH2/EWASG for Modeling Geothermal Reservoirs with Brines and Non-Condensible Gas. *Geothermics*, Vol. 26 (4), pp.437-464.

Flexser, S. (1991). Hydrothermal alteration and past and present thermal regimes in the western moat of Long Valley Cadera (California). *J. Volcanol. and Geotherm. Res*., Vol. 48, pp.303-318.

Henley, R. W., Truesdell, A. H., and Barton, P. B. Jr. (1984). Fluid-Mineral Equilibria in Hydrothermal Systems. *Reviews in Economic Geology,* Vol. 1, Society of Economic Geologists, El Paso, TX.

Johnson J. W., Knauss, K. G., Glassley, W. E., Deloach, L. D., Tompson, A. F. B. (1998). Reactive transport modeling of plug-flow reactor experiments: Quartz and tuff dissolution at 240°C. *J. Hydrol*., 209, pp.81-111.

Moller, N., Greenberg, J. P., and Weare, J. H. (1998). Computer Modeling for Geothermal Systems: Predicting Carbonate and Silica Scale Formation, CO2 Breakout and H2S Exchange. *Transport in Porous Media,* Vol. 33, pp.173 - 204.

Pruess, K. (1991). TOUGH2: A general numerical simulator for multiphase fluid and heat flow. Lawrence Berkeley Laboratory Report LBL-29400, Berkeley, California.

Sorey, M. L. (1985). Evolution and present state of the hydrothermal system in Long Valley Cadera. *J. Geophys. Res*., Vol. 90, pp.11219-11228.

Spycher, N. F. and Reed, M. H. (1989). Evolution of a broadlands-type epithermal ore fluid along alternative P-T paths: Implications for the transport and deposition of base, precious, and volatile metals. *Economic Geology,* Vol. 84, pp.328-359.

Steefel, C. I., and van Cappellen, P. (1990). A new kinetic approach to modeling water-rock interaction: The role of nucleation, precursors and Ostwald ripening. *Geochim. Cosmochim. Acta*, Vol. 54, pp.2657-2677.

Steefel, C. I., and Lasaga, A. C. (1994). A coupled model for transport of multiple chemical species and kinetic precipitation/dissolution reactions with applications to reactive flow in single phase hydrothermal system. *Am. J. Sci.*, Vol. 294, pp.529-592.

Van Genuchten, M. T. (1980). A closed-form equation for predicting the hydraulic conductivity of unsaturated soils, Soil Sci. Soc. Am. J., v. 44, pp.892-898.

Weare, J. H. (1987). Models of Mineral Solubility in Concentrated Brines with Application to Field Observations. *Rev. in Mineralogy,* Vol. 17, pp.143-176.

White, S. P. (1995). Multiphase non-isothermal transport of systems of reacting chemicals, *Water Resour. Res*., Vol. 31, pp.1761-1772.

White, S. P., and Christenson, B. W. (1998). Modeling the Alteration Halo of a Diorite Intrusion. New Zealand Geothermal Congress.

White, S. P., and Mroczek, E. K. (1998). Permeability changes during the evolution of a geothermal field due to the dissolution and precipitation of quartz. *Transport in Porous Media*, Vol. 33, pp.81-101.

White, A. F., and Peterson, M. L. (1990). Role of reactive surface area characterization in geochemical models, In Chemicals Models of Aqueous Systems 2. Amer. Chem. Soc. Symp. Ser., pp.461-475.

White, A. F., and Peterson, M. L. (1991). Chemical equilibrium and mass balance relationships associated with Long Valley hydrothermal system, California, USA. *J. Volcanol. and Geotherm. Res*., Vol. 48, pp.283-302.

Wolery, T. J. (1992). EQ3/6: A software package for geochemical modeling of aqueous systems: Package overview and installation guide (version 7.0). Lawrence Livermore National Laboratory Report UCRL-MA-110662 PT I, Livermore, California.

Xu, T., and Pruess, K. (1998). Coupled modeling of non-isothermal multiphase flow, solute transport and reactive chemistry in porous and fractured media: 1. Model development and validation. Lawrence Berkeley National Laboratory Report LBNL-42050, Berkeley, California, 38 pp.

Table 1. Some parameters used in the simulation for the fracture-matrix system

medium	fracture	matrix	matrix	matrix
symbol	F	M1	M2	M3, M4, M5, M6
grid spacing (m)	0.05	0.1	0.15	0.2, 0.3, 0.4, 0.55
permeability (m^2)	1×10^{-12}	1×10^{-14}	1×10^{-15}	1×10^{-16}
parameters for relative permeability and capillary pressure functions (van Genuchten, 1980):				
λ	0.457	0.457	0.457	0.457
S_{lr}	0.15	0.20	0.30	0.40
S_{ls}	1.0	1.0	1.0	1.0
P_0(pa)	6.195×10^{3}	6.195×10^{4}	1.959×10^{5}	6.195×10^{5}
porosity	0.5	0.1	0.09	0.08
reactive surface reduction factor	1	0.2	0.05	0.01

Table 2. Aqueous chemical concentrations (mol/kg H_2O) of hot reservoir water and cold meteoric water used for the simulation.

Component	hot water	cold water
Ca^{2+}	$4.49x10^{-4}$	$1.27x10^{-4}$
Mg^{2+}	$1.44x10^{-5}$	$2.43x10^{-4}$
Na^{+}	$1.65x10^{-2}$	$1.00x10^{-3}$
K^{+}	$1.23x10^{-3}$	$1.00x10^{-4}$
HCO_3^{-}	$7.92x10^{-3}$	$1.21x10^{-3}$
SO_4^{2-}	$1.86x10^{-3}$	$8.33x10^{-5}$
Al^{3+}	$1.00x10^{-6}$	$1.00x10^{-6}$
SiO_2(aq)	$4.61x10^{-3}$	$9.65x10^{-4}$
Cl^{-}	$7.41x10^{-3}$	$1.61x10^{-4}$
pH	6.6	6.8
T (^{o}C)	225	11

Table 3. Initial rock mineral volume fractions (V_f) and secondary mineral phases (V_f = 0.0) formed in the simulation. Kinetic rate law used is given in Eq.(1). Rate constants are calculated from Eq. (2), and kinetic constant at 25 ^{o}C (k_{25}) and activation energy (E_a) are taken from Steefel and Lasaga [1994], and Johnson et al. [1998].

Mineral	Volume (%)	Surface area (m^2/dm^3 medium)	k_{25} (moles $m^{-2}s^{-1}$)	E_a (KJ/mol)
Primary minerals:				
quartz	35	0.035	$4.30x10^{-14}$	75.00
cristobalite	23	0.023	$3.16x10^{-13}$	69.08
K-feldspar	30	0.03	$1.00x10^{-12}$	67.83
albite	2	0.002	$1.00x10^{-12}$	67.83
anorthite	2	0.002	$1.00x10^{-12}$	67.83
porosity	8	----	----	----
total	100	----	----	----
Secondary minerals:				
kaolinite	0	0.01	$1.00x10^{-13}$	62.76
muscovite	0	0.01	$1.00x10^{-14}$	58.58
pyrophyllite	0	0.01	$1.00x10^{-13}$	62.76
paragonite	0	0.01	$1.00x10^{-14}$	58.58
calcite	0	0.01	$1.00x10^{-11}$	41.87
amorphous silica	0	0.01	$7.94x10^{-13}$	62.80

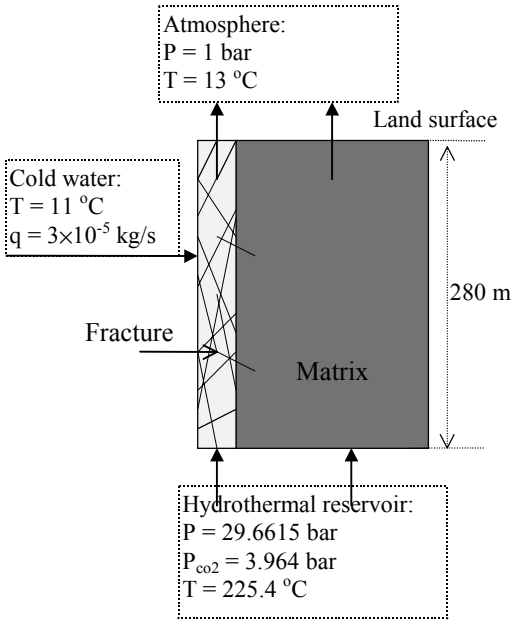

Fig. 1. Vertical 2-D section model for hydrothermal fluid flow and rock alteration in a fractured rock.

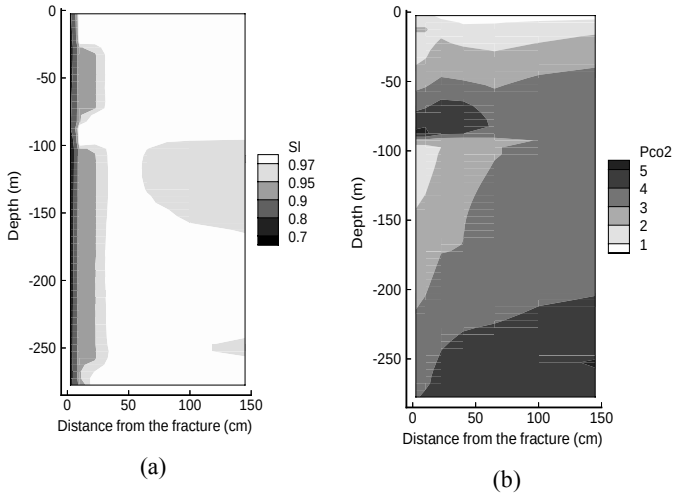

Fig. 2. Steady-state liquid water saturation (a), and CO_2 partial pressure (b, in bar) in the fracture-matrix system without chemical interactions.

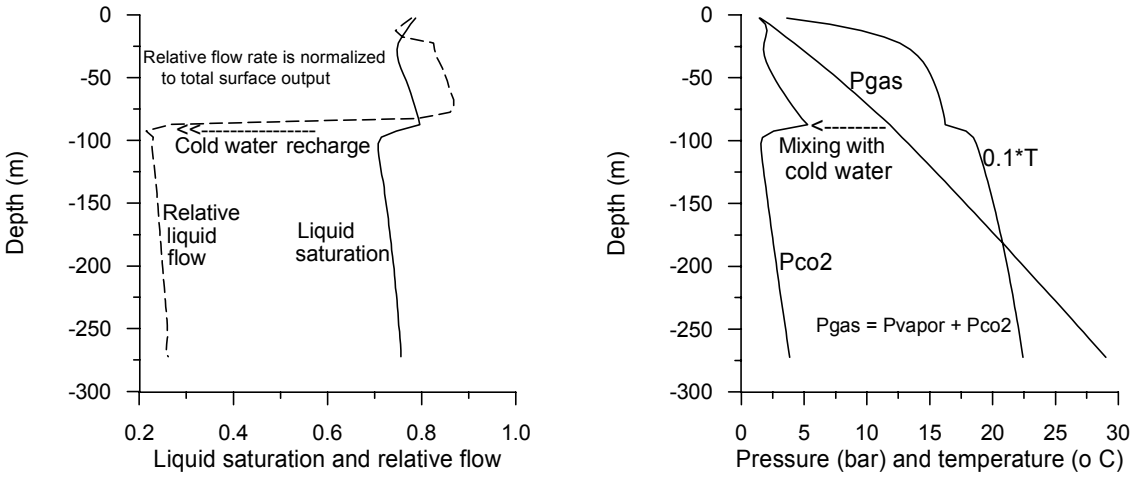

(a) (b)

Fig. 3. Steady-state liquid saturation and relative flow (a), and gas phase pressure and temperature (b) along the fracture in the non-reactive system.

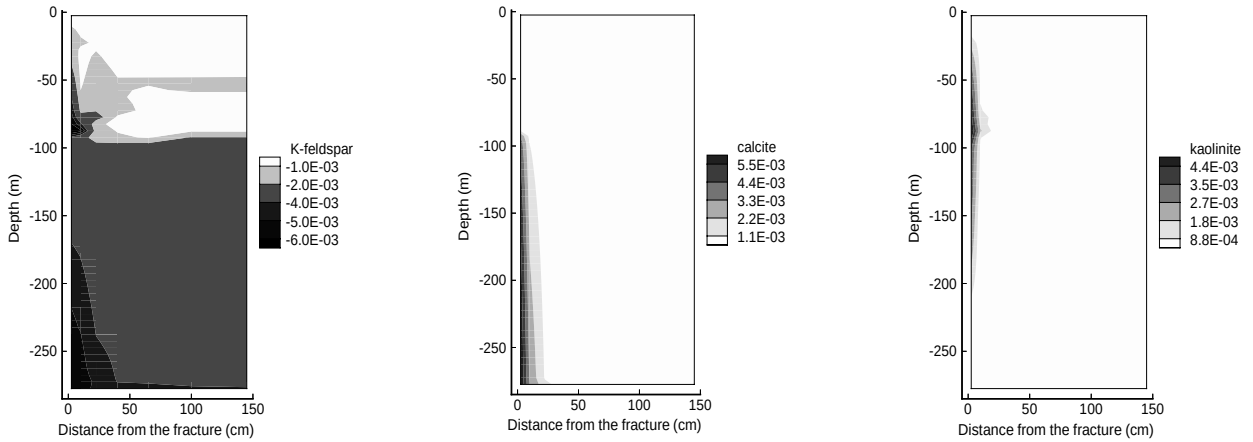

(a) (b) (c)

Fig. 4. Change of mineral abundance (in volume fraction) after 1000 years.

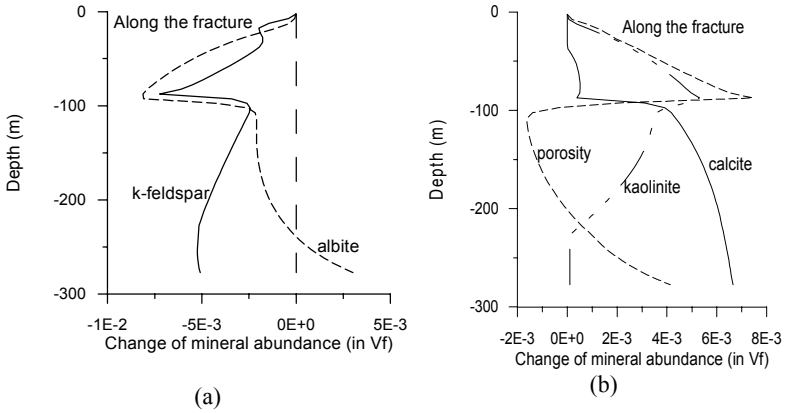

(a) (b)

Fig. 5. Change of mineral abundance (in volume fraction) along the fracture after 1000 years.

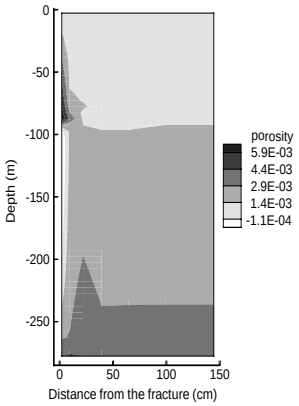

Fig. 6. Change of porosity after 1000 years.